Separation Science and Technology
Publication details, including instructions for authors and subscription information:
http://www.informaworld.com/smpp/title~content=t713708471

Investigations of Performance Characteristics Including Limitations Due to Flow Instabilities in Continuous SPLITT Fractionation

S. Gupta[a]; P. M. Ligrani[b]; J. C. Giddings[c]
[a] DEPARTMENT OF CHEMICAL AND FUELS ENGINEERING, AND DEPARTMENT OF CHEMISTRY FIELD-FLOW FRACTIONATION RESEARCH CENTER, UNIVERSITY OF UTAH, SALT LAKE CITY, UTAH, USA [b] CONVECTION HEAT TRANSFER LABORATORY DEPARTMENT OF MECHANICAL ENGINEERING, MEB 3209, UNIVERSITY OF UTAH, SALT LAKE CITY, UTAH, USA [c] DEPARTMENT OF CHEMISTRY FIELD-FLOW FRACTIONATION RESEARCH CENTER, UNIVERSITY OF UTAH, SALT LAKE CITY, UTAH, USA

To cite this Article Gupta, S. , Ligrani, P. M. and Giddings, J. C.(1997) 'Investigations of Performance Characteristics Including Limitations Due to Flow Instabilities in Continuous SPLITT Fractionation', Separation Science and Technology, 32: 10, 1629 — 1655
To link to this Article: DOI: 10.1080/01496399708000725
URL: http://dx.doi.org/10.1080/01496399708000725

SEPARATION SCIENCE AND TECHNOLOGY, 32(10), pp. 1629–1655, 1997

Investigations of Performance Characteristics Including Limitations Due to Flow Instabilities in Continuous SPLITT Fractionation

SUPRIYA GUPTA
DEPARTMENT OF CHEMICAL AND FUELS ENGINEERING,
AND DEPARTMENT OF CHEMISTRY
FIELD-FLOW FRACTIONATION RESEARCH CENTER

PHILLIP M. LIGRANI*
CONVECTION HEAT TRANSFER LABORATORY
DEPARTMENT OF MECHANICAL ENGINEERING, MEB 3209

J. CALVIN GIDDINGS†
DEPARTMENT OF CHEMISTRY
FIELD-FLOW FRACTIONATION RESEARCH CENTER

UNIVERSITY OF UTAH
SALT LAKE CITY, UTAH 84112, USA

ABSTRACT

An investigation of SPLITT fractionation is conducted to improve its overall performance. Particular attention is devoted to factors which degrade separation resolution in the thin SPLITT channels, including the development of instabilities due to unstable stratification of density. The presence of these instabilities is quantified using the Richardson number (Ri) and the flow-rate ratio $\dot{V}(a)/\dot{V}(a')$, where $\dot{V}(a)$ and $\dot{V}(a')$ are volumetric flow rates at the top outlet substream and the top inlet feed substream, respectively. The stability boundary separating the stable and unstable flow domains is identified in terms of these parameters. Based on these criteria, the region most suitable for operation of SPLITT fractionation corresponds to $\dot{V}(a)/\dot{V}(a') \geq 8$, and Ri in the range of 0.001 to 0.0055, depending upon the value of $\dot{V}(a)/\dot{V}(a')$. Experimental verification is provided by the successful separation of a sample of glass bead particles using a multistage fractionation system.

* To whom correspondence should be addressed.
† Distinguished Professor Cal Giddings passed away on October 24, 1996. We greatly miss our friend, colleague, and mentor.

Key words. SPLITT fractionation; Flow instability; Density stratification; Richardson number

INTRODUCTION

In recent years, numerous analytical techniques have been developed and employed in the separation and characterization of macromolecular, colloidal, and particulate systems. However, most techniques inherently have a small load capacity and are incapable of operating in a continuous mode. This limitation may be critical for many analytical studies which require larger sample amounts for subsequent analysis. In addition, preparative scale separations used for academic and industrial research necessitate systems with high separative capacity.

The resolution of separation techniques such as gravity-driven elutriation and air classification (1, 2) is restricted because of the development of a nonuniform flow profile. Similarly, the performance of electric-field-driven zone electrophoresis (3), isoelectric focusing (4), and isotachophoresis (5) is limited by convection-induced flow distortions. Each of these techniques is also disadvantageous since they involve complex procedures and their response is generally slow and sluggish. Most centrifugal techniques (6) are expensive and involve tedious layering of density gradients to overcome convective perturbations. Other techniques which are particularly suitable for biological samples, such as preparative scale chromatography, lack speed and are cost intensive (7).

A new class of thin flow-cell techniques under development since its inception in 1985 is SPLITT fractionation SF (8). An SF system is illustrated in Figs. 1(a) and 1(b). The channel is thin (300–800 μm) and ribbon-like (aspect ratio > 100) with splitter plates oriented in x–z planes located at each end of the channel. These are designed to split or separate two different flow streams. SF is unique as it utilizes a powerful and generic strategy for rapid and continuous separation of particles in the size range of 0.1 to 100 μm across the thin and precisely controlled flow laminae. By applying different kinds of fields or driving forces across the transverse direction of the cell, particulate as well as macromolecular particles can be separated.

To date, SF has been employed with a variety of different fields/gradients (imposed in the transverse direction) such as gravitational (9, 10), centrifugal (11, 12), electrical (13, 14), crossflow (15), concentration (16, 17), and hydrodynamic lift forces (18). For particles larger than 1 μm, a gravitational field provides good separation. SF systems are advantageous for many analytical (16, 17, 19) and preparative (9, 10) applications be-

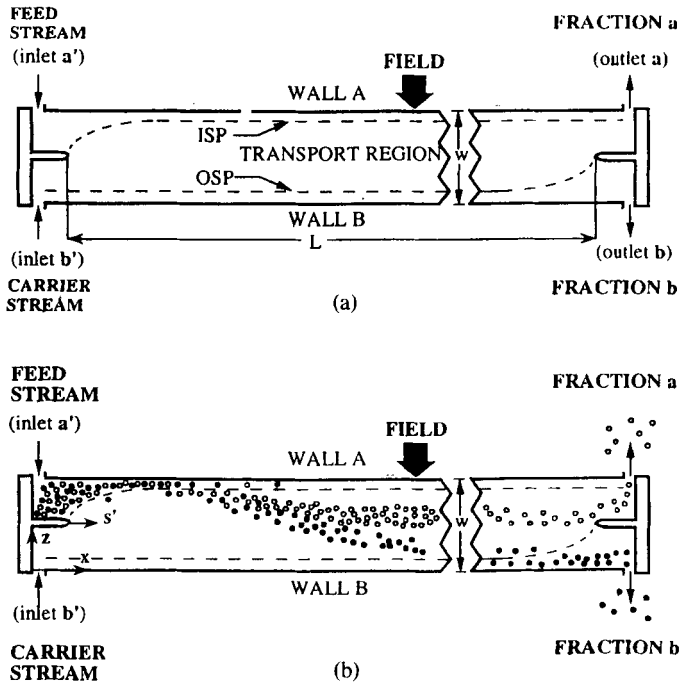

FIG. 1 Schematic (side view) of a gravitational SPLITT channel operated in the uniform transport mode. (a) Transport region. (b) Particle trajectories.

cause of their continuous high speed, high resolution, gentle processing, theoretical tractability, simplicity, and requirement of a relatively inexpensive infrastructure for operation. With the possibility of a scale-up, it is envisioned as an effective sample preparative tool for processing industrial (9, 10, 11), environmental (20), and biological samples (12–14, 21) with sample throughput rates ranging from a few grams to kilograms per hour.

The key to successful separation in SF is uniform laminar flow through the channel. Anything producing a flow perturbation is expected to degrade resolution, including channel imperfections and flow three-dimensionality. The most important channel imperfections include splitter misalignment, surface roughness effects, splitter edge discontinuities, and geometric nonuniformities near both channel ends. Flow three-dimensionality can be induced by instabilities due to unstable density stratification which results when the feed stream has a higher density than the carrier

stream. With the present SF geometry, the density gradient from the stratification occurs at the same flow locations as the shear layer just downstream of the channel inlet. This shear layer results from the different velocities in the carrier and feed streams.

This study focuses on evaluating the limitations on performance and resolution in a thin SPLITT fractionation channel which result when three-dimensionality from unstable density stratification is present. Lower Reynolds numbers ($Re < 2$) than other known investigations of shear layer/density gradient interactions (22, 23) are employed. The effects of the flow-rate ratio $\dot{V}(a)/\dot{V}(a')$ and nondimensional density gradient magnitude on resolution are examined. The overall goal is to determine flow conditions where the operation of SF is stable and can be optimized. Confirmation of good SF performance within the stable region is illustrated by successful separation of a sample of glass bead (GB) particles using a multistage fractionation scheme.

BACKGROUND AND THEORY

Principle of Separation

Operation of an SF system is illustrated by the schematic drawings in Figs. 1(a) and 1(b). As the SF system is started, the sample, which is suspended in a suitable carrier fluid, is continuously introduced through inlet a'. This stream is called the feed substream. Pure carrier fluid (containing no particles) is simultaneously introduced through inlet b'. This is called the carrier substream. Under ordinary operating conditions, flow rates are adjusted such that $\dot{V}(b') > \dot{V}(a')$, which forces the feed stream into a thin lamina close to wall A. The feed lamina is separated from the carrier stream by an imaginary plane referred to as the inlet splitting plane (ISP), as shown in Fig. 1(a). A suitable field, such as a gravitation field, is applied perpendicular to the direction of flow, and this induces vertical displacement of the particles.

Differential displacement of the particles then occurs toward wall B based on the driving force exerted on each particle type by the applied field and the frictional resistance offered by the carrier fluid to particle motion. Thus, different particle types occupy different laminae while the flow through the channel displaces them axially toward the outlet end. Particles mobile enough to cross the second imaginary plane, termed the outlet splitting plane (OSP), exit outlet b (fraction or product b) while the rest exit outlet a (fraction or product a). The OSP eventually joins the outlet splitter plate located at the downstream end of the channel which splits the flow into two substreams which exit outlet a or b.

The region sandwiched between the inlet and outlet splitting planes is called the transport region and functions much like a selective liquid membrane. Differential permeation through this membrane (which leads to separation) is driven by the applied field. The location of the splitting planes and thus the thickness of the transport region control the separation resolution and the cutoff diameter, which is defined shortly. These can be adjusted by altering the positions of the inlet and outlet splitting planes, which is accomplished by regulating the flow-rate ratios either at the channel inlet or the channel outlet.

Theory

The theory for SPLITT fractionation has been elaborated in a number of publications (9). Some relevant features of an SF channel which employ a gravitational field with uniform transport are discussed here.

Differential displacement of particles within the SF channel toward wall B is determined by the particles' sedimentation coefficient. For spherical particles, the sedimentation coefficient is given by

$$s = \frac{(\rho_p - \rho_c)d^2}{18\eta} \tag{1}$$

where ρ_p is the particle density, ρ_c is the carrier density, d is the particle diameter, and η is the carrier viscosity. The particles are assumed to be driven at a constant sedimentation velocity U from wall A to wall B, which is given by

$$U = sG \tag{2}$$

where G is the field-induced acceleration due to gravity. The volumetric flow rate of the transport region $\dot{V}(t)$ is expressed by

$$\dot{V}(t) = \dot{V}(a) - \dot{V}(a') = \dot{V}(b') - \dot{V}(b) \tag{3}$$

where $\dot{V}$ is the volumetric flow rate of a particular stream denoted by the term within parentheses. See Fig. 1. Another important volumetric flow rate is $\Delta\dot{V}$, which is the volumetric flow rate of the lamina across whose thickness a given particle sediments during its transit through the SPLITT channel. This flow rate is given by

$$\Delta\dot{V} = bLU \tag{4}$$

where b is the breadth of the channel and L is the length of the channel. Substituting for U and using Eqs. (1), (2), and (4), one subsequently obtains

$$\Delta\dot{V} = \frac{bL(\rho_p - \rho_c)Gd^2}{18\eta} \tag{5}$$

Under fixed flow conditions in an SF channel, particle population smaller than a certain size d_0 exits entirely from outlet a, the ones larger than another size d_1 exit entirely from outlet b, and the particle population in between these two sizes (d_1 to d_0), which are not fully resolved, exit both outlets in different proportions. For the latter, the fraction of particles of a given size exiting outlet b (or outlet a) can be used as a measure of the separation efficiency. Separation efficiency is quantified using the fractional retrieval parameter F_b or F_a given by the following equations

$$F_b = \frac{\Delta\dot{V} - \dot{V}(t)}{\dot{V}(a')} \tag{6}$$

and

$$F_a = 1 - F_b \tag{7}$$

Combining Eqs. (3), (5), (6), and (7), we get

$$F_a = \frac{\dot{V}(a)}{\dot{V}(a')} - \left[\frac{bL\Delta\rho G}{18\eta\,\dot{V}(a')}\right]d^2 \tag{8}$$

Thus, for a given channel and flow conditions, F_a (and hence F_b) is a function of the particle diameter. A plot of F_a (or F_b) versus the particle diameter is called the recovery plot.

The relative magnitudes of $\Delta\dot{V}$ and $\dot{V}(t)$ indicate whether particles exit the channel through outlet a or b. For particles introduced close to the inlet splitting plane (ISP), particles exit outlet a if

$$\Delta\dot{V} \leq \dot{V}(t)$$

and outlet b if

$$\Delta\dot{V} > \dot{V}(t)$$

The diameter at which 50% of the particles exit outlet b or F_b equals 0.5, and it is called the cutoff diameter, d_c. Substituting $F_b = 0.5$ in Eq. (6) and then using Eqs. (3) and (5), one obtains an equation for the cutoff diameter:

$$d_c = \sqrt{\frac{18\eta[\dot{V}(a) - 0.5\dot{V}(a')]}{bL(\rho_p - \rho_f)G}} \tag{9}$$

From Eq. (9) the cutoff diameter d_c is readily adjusted by controlling the flow rates of streams a and a' for a specified channel geometry. The flow

rates may also be altered by changing the channel dimensions and the carrier viscosity. Once d_c is chosen for a given channel using Eq. (9), the difference between $\dot{V}(a)$ and $0.5\dot{V}(a')$ is fixed. Flow rates $\dot{V}(a)$, $\dot{V}(a')$, $\dot{V}(b)$, and $\dot{V}(b')$ are, however, not uniquely defined by this criteria, and other criteria can then be employed in their selection to further optimize the performance of SF (24). Separation resolution in SF can also be related to channel flow rates using an equation having the form (24)

$$\frac{d_1}{d_1 - d_0} \cong \frac{2\dot{V}(a)}{\dot{V}(a')} \tag{10}$$

According to Eq. (10), the ratio of $\dot{V}(a)$ to $\dot{V}(a')$ allows control of the range of unresolved particles which exit both outlets a and b.

Practical Limitations

One practical limitation encountered in SF concerns the particles leaving the channel from outlet b. Under ordinary operating conditions, this collection of particles, referred to as fraction b, contains only a few of the smaller particles from the top fraction or fraction a, which ideally would exit entirely from outlet a. Thus, SF effectively separates the "oversized" particles (larger than a certain size) from the overall sample, and only a few "undersized" particles (smaller than the specified size) are present as contaminants in fraction b. With this situation, sedimentation drives the particles along the transverse direction, and advection due to forced flow in the channel displaces them longitudinally. Any other secondary flows along the transverse/longitudinal direction are negligible.

As the density of the feed stream becomes somewhat higher than the density of the carrier stream, significant mixing of "oversized" and "undersized" particles in the SF channel occurs. Consequently, particles of all sizes (present in the original sample) exit both outlets a and b, and separation is poor for almost all ranges of particle sizes. Unstable stratification of density in the shear layer between the two streams is responsible for this behavior. This develops secondary flows in the SF channel which seriously degrade separation resolution. Onset of these secondary flows is the principle subject of this investigation.

EXPERIMENTAL APPARATUS, MATERIALS, AND CONDITIONS

Channel

The SPLITT cell construction has been described and illustrated in detail (9), therefore, only a short description will be given here. The pres-

ent SF channel is similar to model SF1000HC from FFFractionation, Inc. of Salt Lake City. Channel dimensions are L = 20 cm, b = 4.0 cm, and w = 635 μm, giving a channel volume of 5.08 mL. The channel thickness is determined by the combined thickness of the two Teflon spacers (254 μm each) and the stainless steel splitter plate (127 μm) sandwiched between the two glass plates which serve as the channel walls. A rectangular section is cut out from the splitter plate which defines the rectangular shape of the SF channel. The ends of both spacers are tapered into triangular shapes, so that the tip of each triangle intercepts the inlet and outlet holes which are drilled through the glass plates.

Instrumentation

The particles in the feed stream are kept well suspended by constant stirring provided by a magnetic stirrer and frequent on-line sonication by a sonicator (Heat Systems Ultrasonic, Inc., Plainview, NY). The experimental setup used in this study is shown in Fig. 2. The feed and carrier solutions are pumped by two independent pumps. The miniplus peristaltic feed pump (Gilson, Inc., Middletown, WI) provides 0.75 mL/min to inlet a' while the carrier pump (QD-0, FMI, Inc., Oyster Bay, NY) provides 5 to 21 mL/min to inlet b'. The flow rates at the two outlets (a and b) are controlled by adjusting the backpressure in the flow lines.

The particle size distributions (PSD) of the two product fractions, discharged from the two outlets of the SPLITT channel, are determined using sedimentation field-flow fractionation (SdFFF). SdFFF is a well-established analytical separation and characterization technique (25) suitable

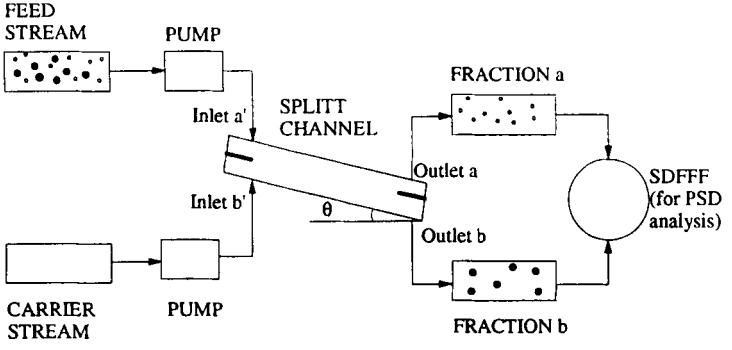

FIG. 2 Gravitational SPLITT channel and ancillary components used in continuous fractionation and PSD analysis of PS latex particles.

for the analysis of macromolecules, colloids, and particulate samples. The SdFFF system used for PSD analysis is in most respects identical to the model S101 Colloid/Particle Fractionator from FFFractionation, Inc. of Salt Lake City. The dimensions of the SdFFF channel are L = 90 cm, b = 2.0 cm, and w = 127 μm. The radius of rotation is 15.1 cm. It is operated at a rotational speed of 1250 rpm. The channel flow rate is maintained at 9.5 mL/min by a model 110B solvent delivery module from Beckman Instruments, Inc. A UV absorbance detector (Spectra 100 from Spectra Physics) is operated at a wavelength of 254 nm and connected to the channel outlet. The sample injection volume is varied from 50 to 100 μL depending on the sample concentration.

Materials

The carrier fluid used in SF and SdFFF is an aqueous solution of 0.1% (w/v) FL-70 detergent (Fisher Scientific, Fair Lawn, NJ) and 0.02% (w/v) sodium azide bacteriocide (Sigma Chemicals, St. Louis, MO). In this study, two different particles are fractionated using SF. These are polystyrene (PS) latex particles with nominal diameters in the size range of 1 to 35 μm and a density of 1.05 g/mL from Duke Scientific (Palo Alto, CA), and glass bead particles in the size range of 5 to 60 μm and a density of 2.44 g/mL. Microscopic examination of the GB particles showed the presence of air bubbles in a few particles which altered their density. As it is essential to have particles of uniform density, a procedure to remove all particles with air bubbles was carried out. The GB particles were suspended in 1,4-diiodobutane (Aldrich, Milwaukee, WI) which has a density of 2.35 g/mL, and all lighter particles which floated on top were removed. To examine the effect of unstable density stratification in SF, the density of the feed (ρ_f) and/or carrier (ρ_c) streams was modified by adding sucrose crystals obtained from Mallincrodt (Chesterfield, MO).

Experimental Conditions

Using SF, PS latex particles are fractionated at different Re, Ri, and d_c. The flow rates [$\dot{V}(a')$, $\dot{V}(b')$, $\dot{V}(a)$], $\Delta\rho/\bar{\rho}$, and the calculated parameters including l', ΔU, Ri, and Re are listed in Table 1 for each cutoff diameter examined. All of these parameters are explained in the next section. Table 2 lists the flow rates employed to effect the separation of glass bead particles at different d_c. Due to the high density of the GB particles (2.44 g/mL) and the large cutoff diameters employed in this study, the required channel flow rate calculated using Eq. (5) is 150 mL/min for d_c = 20 μm. This value is very near the maximum operationally feasible flow rate for our SF channel, which is also about 150 mL/min. Thus, it is essential to

TABLE 1
Flow Conditions Employed for Experiments and FLUENT Calculations

d_c (μm)	$\dot{V}(a')$ (mL/min)	$\dot{V}(b')$ (mL/min)	$\dot{V}(a)$ (mL/min)	$\frac{\Delta\rho}{\bar{\rho}} \times 10^4$	l' (μm)	ΔU (cm/s)	Re	Ri
11.1	0.75	5	1.98	18.9	39.5	0.715	0.28	0.014
				8.12				0.0061
				6.22				0.0047
				2.40				0.0018
20.7	0.75	6.75	6	15.3	38.6	1.01	0.39	0.0057
				10				0.0037
				6.22				0.0023
				2.40				0.0009
25.7	0.75	11	9	30.8	36.3	1.72	0.624	0.0037
				21.3				0.0026
				11.9				0.0014
				8.17				0.0010
29.8	0.75	16	12	77.8	33.3	2.56	0.852	0.0039
				40.2				0.0020
				28.9				0.0014
				21.3				0.0010
34.6	0.75	21	16	77.8	30.9	3.30	1.05	0.0020
				59				0.0015
				47.7				0.0012
				40.3				0.0010

alter a suitable parameter in Eq. (5) so that the total channel flow rate is reduced. As the channel dimensions are fixed, this is accomplished by tilting the channel at an angle which reduces the field-induced acceleration G in Eq. (5) by the cosine of the tilt angle θ (see Fig. 2). Thus, θ is used to regulate the total channel flow rate for each d_c value, as indicated in Table 2.

TABLE 2
Experimental Conditions to Obtain Different Cutoff Diameters (d_c) for the Separation of Glass Bead Particles in a Stable Density Gradient. SPLITT cell used: L = 20 cm, b = 4.0 cm, w = 635 μm

d_c (μm)	$\dot{V}(a')$ (mL/min)	$\dot{V}(b')$ (mL/min)	$\dot{V}(a)$ (mL/min)	Channel tilt angle θ°
20.6	4	81	50	73
31.2	4	130	112	73
40.4	4	156	125	78.5

RESULTS AND DISCUSSION

SPLITT Fractionation Channel Performance Evaluation

The fractional retrieval parameter F_a, mentioned earlier, is the ratio of the number of particles of a given diameter exiting outlet a to the total number of particles in the feed stream. The recovery plot is then the variation of the fractional retrieval parameter with particle diameter. The recovery plot described by Eq. (8) theoretically gives the highest possible values of F_a at each value of particle diameter, d. Experimentally measured F_a closely approach theoretical values (within a few percent at all d) only with the most optimal experimental conditions.

To determine recovery plots from experimental data, the two fractionated product fractions are analyzed (using SdFFF) to determine M_a, the mass amount of a particular particle size which exits outlet a, and M_b, the mass amount of a particular particle size which exits outlet b. F_a is then determined for a specific particle diameter using the equation

$$F_a = \frac{M_a}{M_a + M_b}$$

M_a and M_b are determined for all particle sizes to obtain particle size distributions (PSDs) at flow conditions corresponding to a particular cutoff diameter d_c, specified by Eq. (9). The experimental recovery plot in the form of F_a versus d is subsequently constructed. Examples of such plots are shown in Fig. 3. The deviation between the experimental and theoretical recovery plots is subsequently used to gauge the channel performance and to quantify the separation efficiency. This is discussed in reference to Figs. 3 and 5 shortly.

Characterization of Unstable Density Stratification in SF

Under nominal SF operating conditions with stable channel flow, experimental retrieval is within 10% of theoretical retrieval for all particle sizes. However, under certain operating conditions, fractional retrieval (F_a versus d) is lower when the density of the feed stream is substantially higher than the density of the carrier stream. This is due to unwanted mixing in the channel which distributes particles of all sizes (present in the original sample) so that they exit both outlets a and b, as mentioned. Here, the onset of this mixing is characterized, and its dependence on the density difference between the carrier and feed streams is quantified. These characterizations are strongly dependent upon the physics of the advecting shear layer located at the interface between the feed and carrier streams.

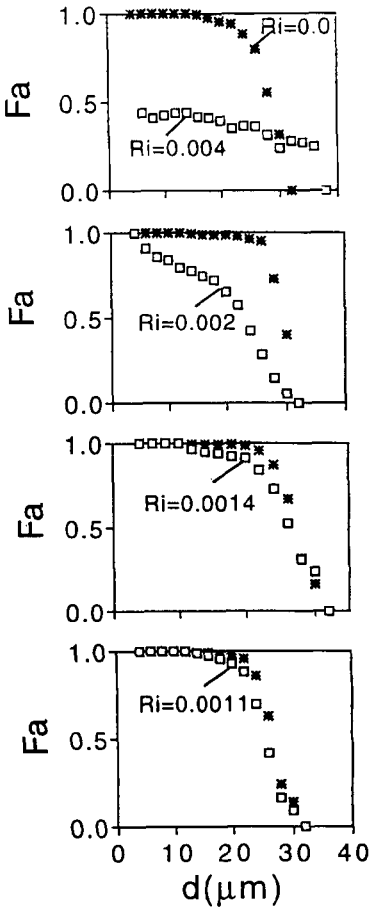

FIG. 3 Recovery plots at 30 μm cutoff diameter. $\dot{V}(a') = 0.75$, $\dot{V}(a) = 12$, $\dot{V}(b') = 16$, $\dot{V}(b) = 4.75$ mL/min.

Investigations of the advection dynamics of particulate suspensions have been described by a number of investigators. Of these, Turner et al. (22) examined the situation when small particles are overlain by a clear fluid whose density is greater than the bulk suspension fluid but less than the density of the interstitial fluid. The settling of the dense suspended particles leads to vigorous advective mixing in the overlaying fluid. Woods et al. (23) conducted similar experiments involving sedimentation below a two-layer stratified region. Their results showed turbulent mixing and

entrainment across the top density interface over a broad range of experimental conditions, which are characterized by the Richardson number.

The dimensionless Richardson number parameter Ri is also used in this study to characterize SF channel mixing which results from the instabilities induced by unstable density stratification. The Ri form employed here is defined as the square of the natural convection velocity scale to the square of the forced convection velocity scale (26). It thus provides a measure of advective buoyancy effects which induce secondary flows in the transverse channel direction (z direction) relative to the forced advection in the axial direction of the channel (x direction). The Richardson number is given by the equation

$$\mathrm{Ri} = \frac{(\Delta\rho/\bar{\rho})Gl'}{\Delta U^2} \tag{11}$$

where $\Delta\rho$ is the density difference between the feed and carrier stream, $\bar{\rho}$ is the average density in the channel, G is the acceleration due to gravity, l' is the characteristic integral length scale, and $\Delta U = U_c - U_f$, where U_c and U_f are the spatially averaged carrier and feed velocities, respectively, at the two SF channel inlets.

The characteristic integral length scale l' employed in the Richardson number provides a measure of the vertical extent of mixing (26). It is determined using an equation having the form

$$l' = (1/\Delta U^2) \int_{z_a}^{z_b} [u_c - u(z)]\,[u(z) - u_f]dz \tag{12}$$

where $u(z)$ is the local streamwise velocity at different transverse locations just downstream of the splitter plate, and u_c and u_f represent the local maximum magnitudes of the velocity distributions in the carrier and feed streams, respectively. The limits of the integral, z_a and z_b, extend from one local velocity maximum to another. The Reynolds number Re is also based on the length scale l' and velocity difference ΔU. It is given by

$$\mathrm{Re} = \frac{\rho l' \Delta U}{\eta} \tag{13}$$

To evaluate l' using Eq. (12), the velocity profile along the transverse direction in the channel $u(z)$ is needed. To obtain $u(z)$, numerical flow simulations are conducted using the FLUENT software (Fluent Inc., Lebanon, NH). Flow simulations are conducted for a channel with $L = 0.15$ mm, $b = 4$ cm, and $w = 635$ μm. The program uses an iterative finite differencing numerical procedure to solve the Navier–Stokes equation governing the fluid flow. As the channel breadth is much greater than

the channel thickness, it is assumed that flow variations along the lateral direction are negligible in comparison to the variations along the transverse direction. Thus, the numerical flow simulations are two-dimensional. They are carried out for all of the experimentally investigated flow conditions indicated in Table 1. For all flow conditions, l' is evaluated using $u(z)$ at a distance 0.06 mm downstream from the splitter plate. At this location, l' is close to the maximum predicted value. Ri and Re are then determined using Eqs. (11) and (13).

To simulate the conditions present in the experiments, the density difference present between the feed and carrier streams must be modeled under isothermal conditions. However, under isothermal conditions, FLUENT lacks the capability to model two single-phase fluid streams with different physical properties such as different fluid density or viscosity. This software limitation is overcome by predicting the characteristics of the two streams at different temperatures to give the same density levels employed in the experiments. The thermal conductivities of the fluids in the FLUENT calculations are determined by equating Prandtl numbers ($\eta c_p/k$) in the numerical calculations to experimental Schmidt numbers ($\eta/\rho D$), where c_p is the specific heat of the fluid, k is the thermal conductivity of the fluid, and D is the diffusion coefficient.

Recovery Plots with Stable and Unstable SF Operating Conditions

Table 1 presents the flow conditions employed to fractionate polystyrene particles at different cutoff diameters and the corresponding FLUENT calculations. Richardson numbers are altered by varying $\Delta\rho$ and/or ΔU. $\Delta\rho$ is varied by adding calculated amounts of sucrose crystals to either or both feed and carrier solutions, and ΔU is varied by varying the carrier stream velocity. All data in Table 1 are obtained for $\rho_f > \rho_c$ or $\mathrm{Ri} > 0$ which correspond to unstable density gradient conditions where secondary flow effects may cause significant mixing within the channel. When $\rho_f < \rho_c$, a stable density gradient is present, channel mixing from secondary flows is negligible, and the Richardson number is set equal to zero.

Recovery plots are determined for all SF flow conditions listed in Table 1. One such set of recovery plots for stable and unstable density gradients at flow rates corresponding to a cutoff diameter of 30 μm is presented in Fig. 3. In each of the four parts of the figure, the recovery plot is obtained at a particular Ri between 0.001 and 0.004 (unstable density gradient) and is compared to the recovery plot for $\mathrm{Ri} = 0$ (stable density gradient). As Ri decreases, differences between the recovery plots for $\mathrm{Ri} > 0$ and $\mathrm{Ri} = 0$ decrease. Physically, this means that flow mixing caused by sec-

ondary flows induced by unstable stratification of density is reduced as the Richardson number decreases. Consequently, a larger percentage of particles are recovered through the two SF outlets in accordance with the theory. Recovery plots obtained at other flow-rate conditions (or cutoff diameters) indicated in Table 1 show similar increases in the secondary flow effects as Ri increases with increasing $\Delta\rho$.

Stability Boundary in SF

To identify the stability boundary which demarcates the stable and unstable flow domains in SF, the effect of the unstable density gradient on channel mixing must be quantified. This is done by evaluating the fractional difference between the areas of recovery plots obtained under stable and unstable density gradients such as the ones shown in Fig. 3. These areas are given by

$$A_{\text{stable}} = \int_{d_{\min}}^{d_{\max}} F_{a,\text{stable}} \mathrm{d}d \tag{14}$$

and

$$A_{\text{unstable}} = \int_{d_{\min}}^{d_{\max}} F_{a,\text{unstable}} \mathrm{d}d$$

respectively. Here, $d_{\max}$ and $d_{\min}$ are the largest and the smallest particle diameters in the feed sample, respectively. The quantitative magnitudes of each integral representing the area under an individual recovery plot is obtained by numerical integration. The fractional difference denoted by parameter R then has the form

$$R = \frac{A_{\text{stable}} - A_{\text{unstable}}}{A_{\text{stable}}}$$

R is a convenient parameter because it provides a relative measure of the separation efficiency under different fractionation conditions.

Magnitudes of R are determined for all flow conditions listed in Table 1 as a function of Ri and flow rates corresponding to different cutoff diameters, d_c. Results showing the variation of R as a function of Ri and d_c are shown in Fig. 4. As Ri increases, a steep increase in R is evident for all values of d_c. Also, the slope of the R versus Ri line increases as d_c is increased. This is because, as d_c is increased, a larger range of particle sizes and thus a larger fraction of the feed sample is recovered through outlet a because larger numbers and size ranges of particles are unable to cross the OSP. Thus, the local density gradient is larger, the flow is more likely to be unstable, and the critical Richardson number at the mixing onset decreases as d_c increases.

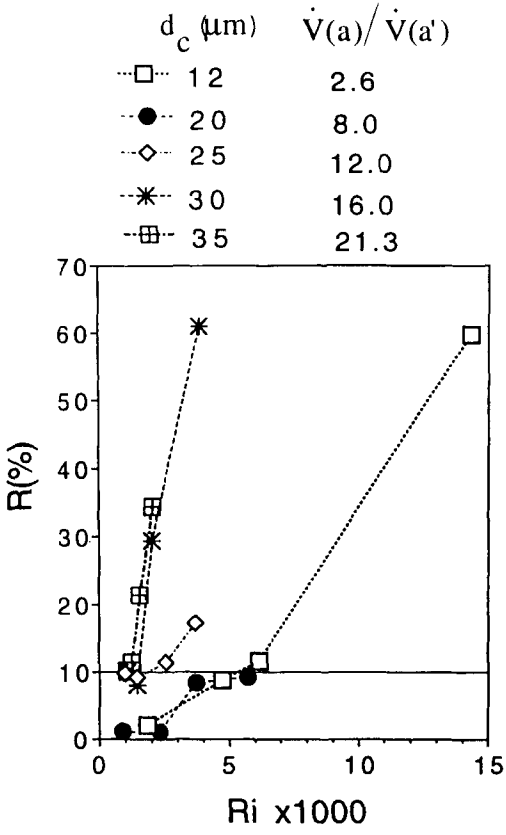

FIG. 4 Variation of R at different cutoff diameters as a function of the Richardson number. $R = 0.1$ locates the critical Richardson number.

The stability boundary is the range of experimental conditions which demarcates the SF channel behavior with no mixing when fractionation is successful from channel behavior when mixing is present and fractionation is unsuccessful. The former condition is considered to be present when A_{unstable} is at least 90% of A_{stable}, which means that 10% or less of the total number of particles remain unfractionated due to mixing. This corresponds to

$$R \leq 0.1 \tag{15}$$

which is identified in Fig. 4. Intersections of the $R = 0.1$ line with lines through experimental data at different d_cs in this figure thus locate corre-

sponding critical Richardson numbers Ri_{cr} on the stability boundary. Critical Richardson numbers thus vary with d_c. The choice of this boundary is sensible since curves showing the variation of R with Ri in Fig. 4 generally show a change in slope as R increases above 0.1. This stability boundary is also verified by additional experiments, including ones involving flow visualization (27, 28).

Effect of the Flow-Rate Ratio $\dot{V}(a)/\dot{V}(a')$ on Separation Resolution

According to Eq. (10), theoretical resolution in SF is enhanced by increasing the flow-rate ratio $\dot{V}(a)/\dot{V}(a')$. This increases the thickness of the transport region or the distance over which particle separation occurs, provided all particles are introduced close to the ISP and thus have the same starting position along the transverse direction. However, in actual practice an unknown distribution of particles exists well above the ISP, resulting in different transverse initial positions for different particles. Because the transportation path over which particle separation occurs in SF is inherently short (~100 μm), variations in the starting positions of different particles can cause the experimental resolution to be different from the theoretical resolution under certain flow conditions.

This difference between the theoretical and experimental resolution is quantified using the parameter R', which is the fractional difference between $A_{\text{theoretical}}$, the area under the theoretical recovery plot given by Eq. (8), and A_{stable} given by Eq. (14). In equation form,

$$R' = \frac{A_{\text{theoretical}} - A_{\text{stable}}}{A_{\text{theoretical}}}$$

where

$$A_{\text{theoretical}} = \int_{d_{\min}}^{d_{\max}} F_{a,\text{theoretical}} \mathrm{d}d$$

Thus, R' is used to quantify resolution when the flow is stable. As such, R' provides an effective measure of a number of factors, including channel imperfections and the spread in the initial distribution of the particles above the ISP, which are responsible for the deviation between the experimental and theoretical resolutions. Deterioration in resolution due to channel imperfections is not a strong function of the channel flow rates. However, the initial spread in the particles above the ISP is a function of the channel flow rates, and thus, variations of R' with flow rates provide an indication of the quantitative influences of this effect.

R' is evaluated over a range of flow conditions which correspond to different values of $\dot{V}(a)/\dot{V}(a')$. Figure 5 shows the variation of R' as a function of $\dot{V}(a)/\dot{V}(a')$. As $\dot{V}(a)/\dot{V}(a')$ decreases, R' increases, indicating increased differences between theoretical and experimental resolution. R' levels off for $\dot{V}(a)/\dot{V}(a') \geq 8$, indicating improved channel performance. Overall, these trends indicate that particle spreading above the ISP is negligible for $\dot{V}(a)/\dot{V}(a') \geq 8$. The behavior illustrated by Fig. 5 is also consistent with Eq. (10) since lower R' indicates better SF channel performance at higher $\dot{V}(a)/\dot{V}(a')$.

Region Favorable for SF Operation

From the quantitative variations of R and R', the range of experimental conditions most favorable for the operation of SF channels is established in terms of Ri and $\dot{V}(a)/\dot{V}(a')$. Experimental data are presented in Fig. 6. The most favorable region for SF channel operation is then at $\mathrm{Ri} < \mathrm{Ri}_{cr}$ (i.e., to the left of the stability boundary), and $\dot{V}(a)/\dot{V}(a') > 8$ (i.e., above the flow-rate ratio limitation line). In the region to the right of the stability boundary, secondary flows due to unstable stratification of density are significant and result in mixing so that particles of different sizes are pres-

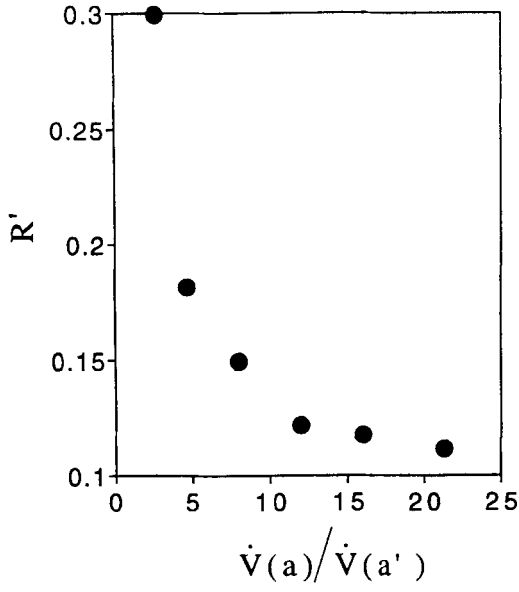

FIG. 5 Variation of R' with $\dot{V}(a)/\dot{V}(a')$.

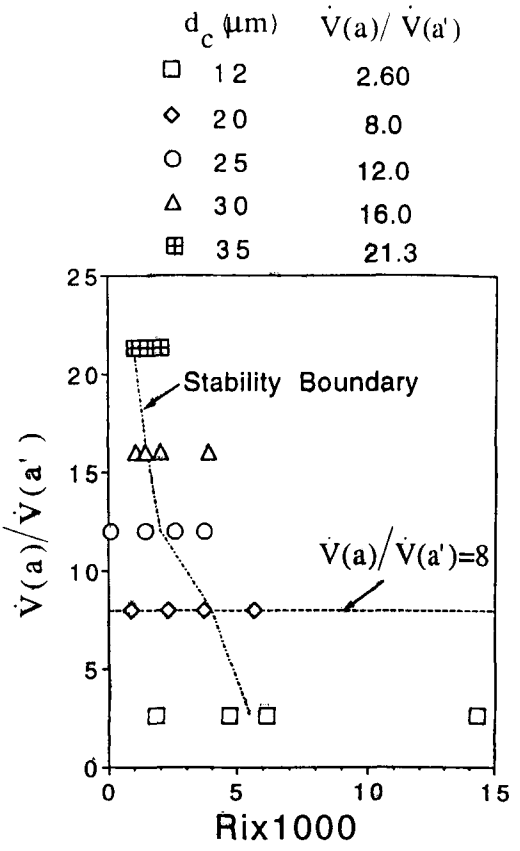

FIG. 6 Variation of $\dot{V}(a)/\dot{V}(a')$ with Ri at various cutoff diameters. Stability boundary and $\dot{V}(a)/\dot{V}(a') = 8$ are also indicated.

ent in the two product streams. This is unsuitable for SF operation. In the region to the left of the stability boundary and below the line corresponding to $\dot{V}(a)/\dot{V}(a') = 8$, deviation between experimental and theoretical resolution is significant even though secondary flow effects may be negligible. Thus, this region is also unsuitable for SF operation.

The stability boundary shown in Fig. 6 is strongly dependent upon the Richardson number with weaker dependence on the channel flow-rate ratio $\dot{V}(a)/\dot{V}(a')$. As d_c increases along with $\dot{V}(a)/\dot{V}(a')$ and Re, the critical Richardson number decreases approximately from 0.0055 to 0.001. When the feed sample is introduced in the channel, it is initially present above

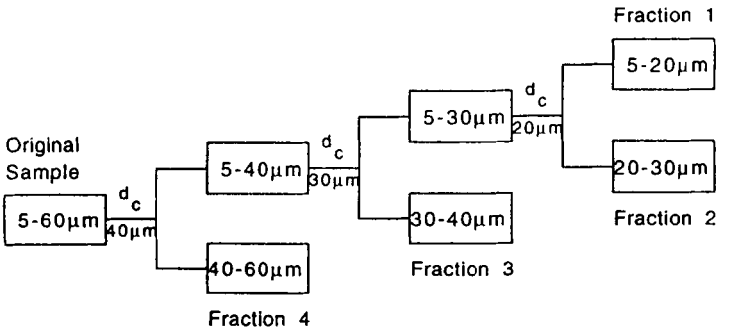

FIG. 7 Multistage fractionation scheme employed in the separation of glass bead particles. For experimental conditions, see Table 2.

the ISP, and the local density gradient is higher than anywhere else in the channel. As time increases, particles then sediment in the traverse direction, density gradients are reduced, and density in the channel is then more uniform at locations closer to the channel outlets. Thus, local and

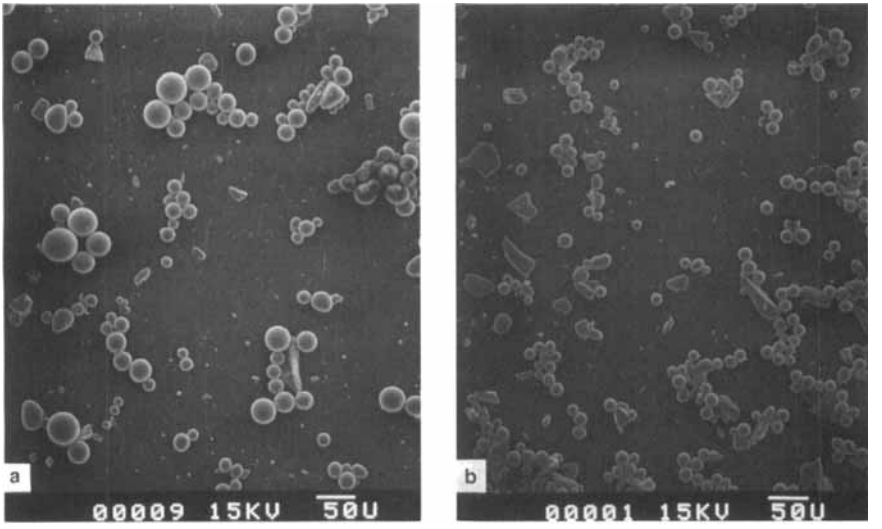

FIG. 8 Micrographs of the original glass bead sample and the four fractionated product fractions under stable density gradient and high resolution conditions. (a) Original sample, d = 5–60 μm. (b) d = 5–20 μm. (c) d = 20–30 μm. (d) d = 30–40 μm. (e) $d > 40$ μm. For experimental conditions, see Table 2.

global density gradients are altered by sedimentation, as well as by the total fraction of particles recovered through outlet b. This fraction is controlled by varying the volumetric flow rates at the channel outlets and inlets, and hence, by varying the particle cutoff diameter. At locations throughout the channel, as d_c increases, a larger range of particle sizes

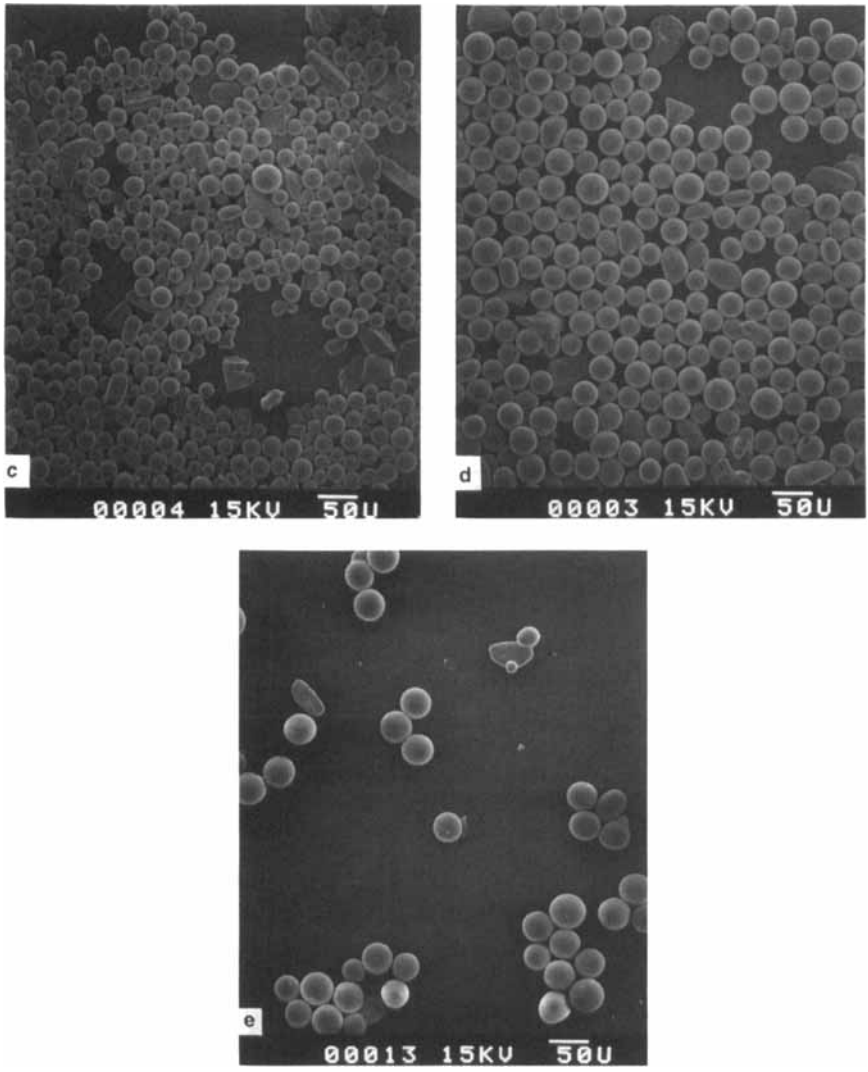

FIG. 8 Continued

(and a larger fraction of the feed sample) are sustained above the OSP, causing the local density gradient to be more unstable, which lowers the critical Richardson number. As d_c is dependent on the flow rates employed, the stability boundary too is flow-rate dependent.

To maintain stable and safe SF channel operation for all flow rates employed in this study, Fig. 6 shows that the Richardson number should always be maintained below 0.001. This limit is based upon the worst possible scenario which could exist in an SF channel when all particles are recovered through outlet a, or when the cutoff diameter is the same as the largest particle diameter in the feed sample. The density gradient in the channel is then highly unstable because, with ideal operation and no mixing, the particles do not cross the OSP. In this situation, unwanted mixing occurs at the lowest possible Richardson number. For the range of conditions covered by our study, particles range in size from 1 to 35 μm, and the condition is met when the cutoff diameter equals 35 μm. The corresponding Ri_{cr} is approximately 0.001, which requires that Ri be maintained less than 0.001 for satisfactory resolution.

With the limits on channel conditions established by Ri_{cr}, the limiting density difference $\Delta\rho$ between the carrier and the feed stream is known, which places bounds on the maximum feed sample concentration. Similarly, the limitation provided by $\dot{V}(a)/\dot{V}(a')$ establishes bounds on the maximum sample throughput rate in SF channels.

Multistage Fractionation of GB Particles

Having identified a region suitable for SF operation, the separation of glass bead (GB) particles is examined under stable density gradient and high resolution conditions. As the density of glass beads is much higher than the density of polystyrene particles, the development of secondary flows due to unstable density stratification places important limitations on sample concentration and hence its throughput. This limitation is overcome by adding sucrose to the carrier stream to produce a stable density gradient. In addition, the flow-rate ratio $\dot{V}(a)/\dot{V}(a')$ is always maintained at values which are greater than 8 to achieve adequate separation resolution.

The feed sample contains GB particles ranging in size from 5 to 60 μm and is separated into four fractions by employing the multistage fractionation scheme shown in Fig. 7. Cutoff diameters equaling 40.4, 31.2, and 20.6 μm are employed in the three successive fractionation stages to yield the four product fractions in the approximate size ranges of 5–20, 20–30, 30–40, and 40–60 μm. The experimental flow conditions and the channel tilt angle at each d_c are indicated in Table 2. The sample throughput in each fractionation stage is approximately 2 g/h. This throughput can be readily increased for other applications by suitably scaling the channel

dimensions. Micrographs of the original feed sample and the four separated fractions obtained using a scanning electron microscope are shown in Fig. 8. In comparison to previously published results (10), these data indicate that the fraction of "undersized" particles in the four separated products is significantly reduced. Thus, these figures not only demonstrate the ability of SF to produce relatively narrow fractions of GB particles for preparative scale separations, but also illustrate the improvements in SF channel performance which are possible in the absence of instabilities due to unstable stratification of density.

CONCLUSIONS AND SUMMARY

Performance of SPLITT fractionation is enhanced by proper selection of channel flow rates and by manipulating the density difference between the carrier and feed streams to decrease secondary flow effects due to unstable density stratification. The boundary which separates the stable and unstable experimental domains is important because it also separates regions corresponding to satisfactory and unsatisfactory resolution in SPLITT fractionation channels.

The stability boundary is characterized in terms of the Richardson number of which it is a strong function. The stability boundary is also dependent upon the channel Reynolds number and the flow-rate ratio $\dot{V}(a)/\dot{V}(a')$. In the experiments conducted, as $\dot{V}(a)/\dot{V}(a')$ is increased from 2.6 to 21.3, the critical Richardson number varies between 0.0055 and 0.001. However, a "safe" region independent of the flow conditions employed is achieved when the Richardson number is less than 0.001. An additional constraint is imposed by the flow-rate ratio $\dot{V}(a)/\dot{V}(a')$ which must be greater than 8 to give satisfactory separation resolution.

Optimal resolution can be obtained in many applications by modifying the carrier density by adding a suitable chemical or by altering the temperature of the feed or carrier stream suitably. This is demonstrated by successful fractionation of GB particles in a multistage SF fractionation system with stable density gradients and high values of $\dot{V}(a)/\dot{V}(a')$. The results from this procedure not only show the improvements in separation resolution which result in the absence of secondary flows induced by unstable density stratification, but also provide evidence of the potential of SF for a wide range of preparative scale separations.

ACKNOWLEDGMENT

The authors acknowledge support for this project from NSF Grant CHE-9322472.

GLOSSARY

a	top outlet of the channel
a'	feed inlet
A_{stable}	area of recovery plot under stable density gradient conditions
A_{unstable}	area of recovery plot under unstable density gradient conditions
$A_{\text{theoretical}}$	area of theoretical recovery plot
b	channel breadth
b	bottom outlet of the channel
b'	carrier inlet
c_p	specific heat of fluid
D	diffusion coefficient
d	particle diameter
d_1	particle diameter for which $F_b = 1$
d_0	particle diameter for which $F_a = 0$
d_c	cutoff diameter
d_{max}	largest particle diameter in the feed sample
d_{min}	smallest particle diameter in the feed sample
F_a	fraction of particles retrieved from outlet a at a given diameter
F_b	fraction of particles retrieved from outlet b at a given diameter
G	field-induced acceleration
k	thermal conductivity of fluid
l'	characteristic integral length scale
L	channel length
M	relative mass in arbitrary units
r	channel radius
R	fractional difference between the areas of the recovery plots obtained with stable and unstable density gradients
R'	fractional difference between the areas of the theoretical recovery plot and the recovery plot with stable density gradient
s	sedimentation coefficient
u	local streamwise velocity
u_c	local maximum velocity of carrier stream
u_f	local maximum velocity of feed stream
U	particle sedimentation velocity
U_c	spatially averaged carrier velocity
U_f	spatially averaged feed velocity

$\dot{V}$	total volumetric flow rate through the channel
$\dot{V}(a)$	volumetric flow rate exiting outlet a
$\dot{V}(a')$	volumetric flow rate entering inlet a'
$\dot{V}(b)$	volumetric flow rate exiting outlet b
$\dot{V}(b')$	volumetric flow rate entering inlet b'
$\dot{V}(t)$	volumetric flow rate through transport region
w	channel thickness
ΔU	$U_c - U_f$
η	fluid viscosity
$\Delta\rho$	density difference between the feed and the carrier streams
$\bar{\rho}$	average density in the channel
ρ_c	density of the carrier stream
ρ_f	density of the feed stream
ρ_p	density of the particle
ρ	density of the fluid
θ	channel tilt angle

Abbreviations

GB	glass bead
ISP	inlet splitting plane
OSP	outlet splitting plane
PS	polystyrene
Re	Reynolds number
Ri	Richardson number
Ri_{cr}	critical Richardson number
rpm	revolutions per minute
SF	SPLITT fractionation

REFERENCES

1. R. H. Snow and T. Allen, "Effectively Measure Particle-Size-Classifier Performance," *Chem. Eng. Prog.*, pp. 29–33 (May 1992).
2. T. C. Preltow and T. P. Preltow, "Centrifugal Elutriation (Counter-Streaming Centrifugation) of Cells," *Cell Biophys.*, *1*, 195–210 (1979).
3. S. Ostrach, "Convection in Continuous-Flow Electrophoresis," *J. Chromatogr.*, *140*, 187 (1977).
4. P. G. Righetti, *Isoelectric Focusing: Theory, Methodology, and Applications*, Elsevier Biomedical, Amsterdam, 1983.
5. F. M. Everaerts, J. L. Beckers, and Th. P. E. M. Verheggen, *Isotachophoresis. Theory, Instrumentation, and Applications* (J. Chromatogr. Library, Vol. 6), Elsevier, Amsterdam, 1976.
6. C. A. Price, *Centrifugation in Density Gradients*. Academic Press, New York, NY 1988.

7. G. Guiochon and H. Colin, "Theoretical Concepts and Optimization in Preparative Scale Liquid Chromatography," *Chromatogr. Forum*, p. 21 (Sept.–Oct. 1986).
8. J. C. Giddings, "A System Based on Split-Flow Lateral-Transport Thin (SPLITT) Separation Cells for Rapid and Continuous Particle Separation," *Sep. Sci. Technol.*, *20*, 749–768 (1985).
9. S. R. Springston, M. N. Myers, and J. C. Giddings, "Continuous Particle Fractionation Based on Gravitational Sedimentation in Split-Flow Thin Cells," *Anal. Chem.*, *59*, 344–350 (1987).
10. Y. Gao, M. N. Myers, B. N. Barman, and J. C. Giddings, "Continuous Fractionation of Glass Microspheres by Gravitational Sedimentation in Split-Flow Thin (SPLITT) Cells," *Part. Sci. Technol.*, *9*, 105–118 (1991).
11. C. B. Fuh, M. N. Myers, and J. C. Giddings, "Centrifugal SPLITT Fractionation: New Technique for Separation of Colloidal Particles," *Ind. Eng. Chem. Res.*, *33*, 355–362 (1994).
12. C. B. Fuh and J. C. Giddings, "Isolation of Human Blood Cells, Platelets, and Plasma Proteins by Centrifugal SPLITT Fractionation," *Biotechnol. Prog.*, *11*, 14–20 (1995).
13. J. C. Giddings, "Continuous Separation in Split-Flow Thin (SPLITT) Cells: Potential Applications to Biological Materials," *Sep. Sci. Technol.*, *23*, 931–943 (1988).
14. S. Levin, M. N. Myers, and J. C. Giddings, "Continuous Separation of Proteins in Electrical Split-Flow Thin (SPLITT) Cell with Equilibrium Operation," *Ibid.*, *24*, 1245–1259 (1989).
15. J. C. Giddings, "Crossflow Gradients in Thin Channels for Separation by Hyperlayer FFF, SPLITT Cells, Elutriation, and Related Methods," *Ibid.*, *21*, 831–843 (1986).
16. P. S. Williams, S. Levin, T. Lenczycki, and J. C. Giddings, "Continuous SPLITT Fractionation Based on a Diffusion Mechanism," *Ind. Eng. Chem. Res.*, *31*, 2172–2181 (1992).
17. S. Levin et al., "Analytical SPLITT Fractionation in the Diffusion Mode Operating as a Dialysis Like System Devoid of Membrane: Application to Drug-Carrying Liposomes," *Anal. Chem.*, *65*, 2254–2261 (1993).
18. J. C. Giddings, "Continuous Particle Separation in Split-Flow Thin (SPLITT) Cells Using Hydrodynamic Lift Forces," *Sep. Sci. Technol.*, *23*(1–3), 119–131 (1988).
19. C. B. Fuh, S. Levin, and J. C. Giddings, "Analytical SPLITT Fractionation: Rapid Particle Size Analysis and Measurement of Oversized Particles," *Anal. Chem.*, *64*, 3125–3132 (1992).
20. R. G. Keil, E. Tsamakis, C. B. Fuh, J. C. Giddings, and J. I. Hedges, "Mineralogical and Textural Controls on the Organic Composition of Coastal Marine Sediments: Hydrodynamic Separation Using SPLITT Fractionation," *Geochim. Cosmochim. Acta*, *58*, 879–893 (1994).
21. S. Levin and J. C. Giddings, "Continuous Separation of Particles from Macromolecules in Split-Flow Thin (SPLITT) Cells," *J. Chem. Tech. Biotechnol.*, *50*, 43–56 (1991).
22. Turner et al., "Convection and Particle Entrainment Driven by Differential Sedimentation," *J. Fluid Mech.*, *226*, 349–369 (1991).
23. Woods et al., "On Convection and Mixing Driven by Sedimentation," *Ibid.*, *285*, 165–180 (1995).
24. J. C. Giddings, "Optimization of Transport-Driven Continuous SPLITT Fractionation," *Sep. Sci. Technol.*, *27*, 1489–1504 (1992).
25. J. C. Giddings, M. H. Moon, P. S. Williams, and M. N. Myers, "Particle Size Distribution by Sedimentation/Steric FFF: Development of a Calibration Procedure Based on Density Compensation," *Anal. Chem.*, *63*, 1366–1372 (1991).

26. D. S. Schowalter, C. W. Van Atta, and J. C. Lasheras, "A Study of Streamwise Vortex Structure in a Stratified Shear Layer," *J. Fluid Mech.*, *281*, 247–291 (1994).
27. P. M. Ligrani, S. Gupta, and J. C. Giddings, "Onset and Effects of Instabilities from Unstable Stratification of Density on Mass Transfer in Channel Shear Layers at Low Reynolds Numbers," *Int. J. Heat Mass Transfer*, Submitted, 1996.
28. S. Gupta, P. M. Ligrani, and J. C. Giddings, "Characteristics of Flow Instabilities from Unstable Stratification of Density in Channel Shear Layers at Low Reynolds Numbers," *Ibid.*, Submitted, 1996.

Received by editor May 17, 1996
Revision received November 1996